Physical Met. & Corr. Sect
B.3

AAEC/TM601

AAEC/TM601

AUSTRALIAN ATOMIC ENERGY COMMISSION

RESEARCH ESTABLISHMENT
LUCAS HEIGHTS

CORROSION RESISTANCE OF SOME ALPHA-DISPERSOID ZIRCONIUM ALLOYS IN WATER VAPOUR AT 400°C AND 500°C

by

T.E.CLARE

September 1971

ISBN 0 642 99440 4

AUSTRALIAN ATOMIC ENERGY COMMISSION

RESEARCH ESTABLISHMENT

LUCAS HEIGHTS

CORROSION RESISTANCE OF SOME ALPHA-DISPERSOID ZIRCONIUM ALLOYS IN WATER VAPOUR AT 400°C AND 500°C

by

T. E. CLARE

ABSTRACT

The corrosion of Zr, Zircaloy-4, Zr + 2.5 Nb, Zr + 1.15 Cr + 0.1 Fe and experimental binary alloys of Zr with Cu, Ni, Fe and Cr was studied at 400° and 500°C in moist helium.

The volume fraction of the second phase in the experimental alloys was approximately constant but the distribution and size of the second phase varied slightly from alloy to alloy. Nevertheless, the corrosion behaviour of the alloys was correlated with composition and solute distribution after corrosion, assuming similar metallurgical structures.

No alloying addition significantly improves the corrosion resistance of pure Zr at 400°C though Ni and Cu improve it at 500°C.

The order of increasing corrosion resistance prior to transition appears to follow the order of decreasing alloy solubility in the oxide film. The time to transition and corrosion rate after transition are also related to alloy solubility in the oxide film.

continued ...

ABSTRACT (continued)

Zircaloy-4, Zr + 2.5 Nb and Zr-Cr alloys may not be suitable for service in moist atmospheres at 400-500°C, whereas Zr-Cu, Zr-Fe and Zr-Ni alloys show superior corrosion resistance under these conditions.

National Library of Australia card number and ISBN 0 642 99440 4

The following descriptors have been selected from the INIS Thesaurus to describe the subject content of this report for information retrieval purposes. For further details please refer to IAEA–INIS–12 (INIS: Manual for Indexing) and IAEA–INIS–13 (INIS: Thesaurus) published in Vienna by the International Atomic Energy Agency.

[01] ANNEALING; CHEMICAL REACTION KINETICS; CORROSION RESISTANCE; HIGH TEMPERATURE; OXIDATION; STEAM; WEIGHT; ZIRCONIUM

[02] ANNEALING; CHEMICAL REACTION KINETICS; CORROSION RESISTANCE; HIGH TEMPERATURE; NIOBIUM ALLOYS; OXIDATION; STEAM; WEIGHT; ZIRCALOY; ZIRCONIUM BASE ALLOY

[03] ANNEALING; CHEMICAL REACTION KINETICS; CHROMIUM ALLOYS; CORROSION RESISTANCE; GRAIN SIZE; HIGH TEMPERATURE; IRON ADDITIONS; MECHANICAL PROPERTIES; OXIDATION; STEAM; WEIGHT; ZIRCONIUM BASE ALLOY

[04] ANNEALING; CHEMICAL REACTION KINETICS; CORROSION RESISTANCE; COPPER ADDITIONS; GRAIN SIZE; HIGH TEMPERATURE; INTERMETALLIC COMPOUNDS; MECHANICAL PROPERTIES; OXIDATION; PHASE DIAGRAMS; STEAM; WEIGHT; ZIRCONIUM BASE ALLOY

[05] ANNEALING; CHEMICAL REACTION KINETICS; CORROSION RESISTANCE; GRAIN SIZE; HIGH TEMPERATURE; INTERMETALLIC COMPOUNDS; MECHANICAL PROPERTIES; NICKEL ADDITIONS; OXIDATION; PHASE DIAGRAMS; STEAM; WEIGHT; ZIRCONIUM BASE ALLOY

[06] ANNEALING; BERYLLIUM ADDITIONS; CHEMICAL REACTION KINETICS; CORROSION RESISTANCE; HIGH TEMPERATURE; INTERMETALLIC COMPOUNDS; OXIDATION; PHASE DIAGRAMS: STEAM WEIGHT; ZIRCONIUM BASE ALLOY

[07] ANNEALING; CHEMICAL REACTION KINETICS; CORROSION RESISTANCE; GRAIN SIZE; HIGH TEMPERATURE; INTERMETALLIC COMPOUNDS; IRON ADDITIONS; MECHANICAL PROPERTIES; OXIDATION; PHASE DIAGRAMS; STEAM; WEIGHT; ZIRCONIUM BASE ALLOY

[08] ANNEALING; CHEMICAL REACTION KINETICS; CHROMIUM ALLOYS; CORROSION RESISTANCE; GRAIN SIZE; HIGH TEMPERATURE; INTERMETALLIC COMPOUNDS; MECHANICAL PROPERTIES; OXIDATION; PHASE DIAGRAMS; STEAM; WEIGHT; ZIRCONIUM BASE ALLOY

CONTENTS

continued ...

CONTENTS (continued)

1. INTRODUCTION

In reviews of zirconium alloy development (1, 2) it is generally agreed that, for corrosion in moist atmospheres, zirconium alloys containing Sn or Nb are inferior to those containing Cr, Cu, Fe or Ni. This second group of binary alloy systems are of the eutectoid/eutectic type in which Cr, Cu, Fe and Ni are effectively insoluble in α-zirconium and exist as second phase particles (3). There is much conjecture about the part, if any, these particles play in the corrosion of zirconium alloys. Divergent results on the corrosion of alloys with the same composition are not uncommon and probably arise from a susceptibility to small variations in distribution of the solute concentrated particles. Although metallurgical structure can affect corrosion resistance, it appears that structurally similar Zr-Cr, Cu, Fe and Ni alloys have never been systematically investigated.

By using a favourable combination of composition, transformation schedule and heat treatment this study sought to produce binary alloys with equal volume fractions and similar distribution and morphology of intermetallic particles. A short supplementary study using X-ray line broadening and hardness measurements was carried out to define the annealing characteristics of the alloys and hence ensure that their annealed condition was the same prior to evaluation by corrosion and mechanical testing.

From the corrosion and supporting studies, it was hoped that:

(i) An improved understanding would be gained of the response of corrosion resistance and mechanical properties to zirconium alloy composition.

(ii) A zirconium alloy would be found that would have better corrosion resistance in moist atmospheres at 400°C and 500°C than some of the zirconium alloys developed over the last 20 years.

Experimental binary alloys of Zr-Be, Zr-Cr, Zr-Cu, Zr-Fe and Zr-Ni were compared with each other and with 'pure' Zr, Zircaloy-4, Zr-2.5 Nb and Zr + 1.15 Cr + 0.10 Fe. Other experimental eutectic/eutectoid type binary zirconium alloys were not considered for reasons of neutron economy (Zr-Co, Zr-B, Zr-Mn, Zr-Ag) (4), difficulties in fabrication (Zr-W) (4) or difficulties in microstructural control (Zr-V, Zr-Mo) (5).

2. EXPERIMENTAL PROCEDURE

2.1 Composition

Published data on the equilibrium phase diagrams and the crystallography of the zirconium rich intermetallic phases of the Zr-Be (6-8), Zr-Cr (9-11), Zr-Cu (12-15), Zr-Fe (16-19) and Zr-Ni (20,21) systems are not always in complete

agreement. Figures 1-5 show Zr rich portions of the phase diagrams and Table I lists crystallographic data for the Zr rich intermetallics selected from the above references.

Following the success of a Zr + 1.15 Cr + 0.10 Fe alloy (22), ('Valoy') as a corrosion resistant alloy it seemed reasonable for purposes of comparison to select experimental alloys containing the same vol. per cent intermetallic as this alloy.

By assuming no solid solubility of Cr and Fe in alpha-zirconium and knowing the crystal structure, volume of the unit cell, number of molecules in the unit cell and hence the density of $ZrCr_2$ and Zr_2Fe, the alloy Valoy was calculated to contain approximately 2.12 vol. per cent of intermetallics in a fully annealed condition. The appropriate compositions of the experimental alloys were calculated from the data in Table I, and their compositions together with analyses of the four control alloys are given in Table II.

2.2 Fabrication

All alloys, including the controls, were arc melted as 200 g buttons from iodide zirconium and spectrographically pure alloying additions. They were melted six times, inverting between melts. The buttons were canned in mild steel under 250 mm pressure of argon and hot-rolled at 790°C to sheet approximately 0.050 in. thick. The steel sheath was easily peeled away from the rolled alloy after guillotining along the edges. Each alloy sheet was cleaned in a mixture of $HNO_3/H_2O/HF$ then β-solution treated for six hours at 950°C in vacuum ($< 10^{-5}$ mm Hg), water quenched, cleaned by sand blasting and etching, and cold-rolled 20 per cent (i.e. to 80 per cent of its thickness) at 5 per cent per pass. Part of the sheet was annealed for 24 hours at 565°C (standard for Valoy (22)) and used for initial corrosion tests, and another part was used for annealing studies.

2.3 Corrosion Tests

Coupons (15 mm x 15 mm) were etched in a $HNO_3/H_2O/HF$ mixture, thoroughly washed and dried, weighed and measured and their surface areas determined. Two coupons from each alloy were suspended on nimonic wires in a horizontal tube furnace with a 1.5 in. dia. recrystallised alumina work tube and a 3 in. long uniform hot zone (± 5°C). The furnace work tube was first evacuated by an oil diffusion pumping system to a pressure of 10^{-4} mm Hg. A gas mixture containing 92 mm H_2O + 668 mm He was then admitted to a pressure of 760 mm and a dynamic flow of 20 cm^3/min was maintained through the system. Water vapour was added to the helium by bubbling it through a rapidly stirred vessel containing de-ionised water at a controlled temperature of 50°C. The furnace was heated to 400 or 500°C and after suitable time intervals the furnace was cooled to room temperature and the specimens removed for re-weighing. The positions of the

coupons were systematically changed between successive weighings.

2.4 Annealing Studies

Two coupons (10 mm x 7 mm) from each β-quenched and cold-rolled alloy sheet were etched and then α-annealed in vacuum ($< 10^{-5}$ torr) for 0.5, 1.5, 6, 18, 48 and 120 hours at 450, 550, 650 or 750°C and for 18 hours at 250 and 350°C. The annealed coupons were lightly etched and the hardness in the rolling plane was measured, using a standard Vickers hardness tester with a 10 kg load. Hardness numbers quoted are an average of eight separate impressions.

Metallographic examinations and measurements of X-ray line broadening were restricted to coupons annealed for 18 hours, because it was considered that these would provide sufficient supporting information on recrystallisation and grain growth to obtain an adequate picture of the annealing process for each alloy and to indicate any gross differences. For metallographic observations a section in the rolling direction of the sheet was diamond polished and etched in a $HNO_3/H_2O/HF$ mixture. Two stage cellulose acetate and carbon/platinum shadowed replicas were prepared for electron microscopy, and the volume fraction of precipitates was estimated from electron photomicrographs by making a particle size analysis of 1,000-2,000 particles in each alloy in the Zeiss TGZ3 particle size analyser. X-ray diffraction measurements were made with a Philips diffractometer, employing Ni filtered Cu radiation and rotating the proportional counter about an axis in the plane of the sheet and perpendicular to the rolling direction. The method adopted by Gray (23) was used to determine the line width of the (213)Kα doublet; the peak half-width was measured on the low angle side at half maximum intensity.

2.5 Tensile Tests

Tensile tests were performed on an Instron testing machine with autographic recording, at a cross-head speed of 0.05 in/min.

2.6 Electron Beam Microprobe Analysis and Metallography of Oxidised Alloys

Sections of coupons corroded at 500°C were mounted with vacuum impregnation in a cold setting epoxy resin and polished with γ-alumina. Photomicrographs were taken, and the polished and un-etched surface was then vapour coated with a film of carbon and examined by means of an A.R.L. microprobe. Specimens were examined under identical settings and characteristic X-ray images and linear traces were made.

3. RESULTS

Plots of the log of weight gain vs. the log of time are given in Figures 6 and 7; for clarity the experimental points are given for some curves only. The temperature control of the furnace operating at 400°C failed after 1,000 hours

and the test was discontinued. A second series of coupons tested at this temperature produced slightly higher weight gains than the first series although weight gains and corrosion rates converged after longer exposure times. The data plotted in Figures 6 and 7 are from the second series. For the plots of Figures 6 and 7 the weight gain prior to a rate transition is given by the expression

$$W = k_1 t^{n_1} ,$$

and after the rate transition by the expression

$$W = k_1 t_o^{n_1} + k_2 (t - t_o)^{n_2}$$

where W = specific weight gain
t = time
t_o = time at transition
n_1 = slope of line in pre-transition period
n_2 = slope of line in post-transition period.

The complete corrosion results are given in Table III.

Hardness and the X-ray line width of the (213)Kα doublet are plotted in Figure 8 for some β-quenched and 20 per cent cold-rolled alloys annealed for 18 hours at different temperatures. The general features of these plots are similar for all alloys. Hardness is not changed below approximately 400°C whereas the X-ray line width has decreased 30-50 per cent at this temperature. Low temperature X-ray recovery is usually associated with the re-arrangement of point defects and dislocations and the significant softening between 450 and 650°C is associated with metallographic evidence for recrystallisation (23), some examples of which are given in Figure 9. In all alloys (except the Zr-Be alloy, which contains very large precipitates and is not shown in Figure 9) the β-quenched structure appears to be 'martensitic' with no evidence of intermetallic precipitates. Breakdown of this structure occurs as the annealing temperature increases, and the extensive intermetallic precipitation is shown in the electron photomicrography of Figure 10.

The results of particle size analyses on enlarged transparencies from several electron micrographs similar to those in Figure 10 are given in Table IV. The difference between measured and calculated values for the volume fractions of precipitates is fairly high in some cases, but because the extent of etching must influence the measured values, coincidence of the two values would be fortuitous. Etching might be expected to have the same influence in all cases (that is, all measured values should be larger than the calculated or vice versa). However, in only one alloy (Zr-Ni) is the measured value significantly lower than

the calculated value, but this alloy etched differently to other alloys (Figure 10) and accurate measurements were more difficult.

Results of characteristic electron microprobe X-ray line scans and characteristic X-ray images across sections of oxidised coupons are shown in Figure 11 to illustrate the solute distribution between zirconium alloys and the oxide films formed at 500°C. Tensile properties of the annealed alloys are given in Table V.

4. DISCUSSION

There are only small differences between the corrosion properties of all alloys in the pre-transition period. A narrow band can be drawn to envelop the curves of Zr-Cr, Zr-Cu, Zr-Ni and Zr-Fe alloys, the curves for Zr and Zr-Be lie just below this and those for Zircaloy-4 and Zr-2.5 Nb lie just above. However, zirconium alloys would normally be in service well beyond their rate transition period and the time to transition and the post-transition corrosion rate therefore are of major interest. At 400°C and 500°C Zircaloy-4 and Zr-2.5 Nb show early rate transitions. Valoy, Zr-1.15 Cr, Zr-0.53 Fe and Zr-0.24 Be show rate transitions after intermediate times but Zr-0.56 Cu and Zr-0.58 Ni do not show a rate transition even after 8,000 hours exposure at 400°C and only after 5,000 hours at 500°C. No alloying addition significantly improves the corrosion resistance of pure zirconium at 400°C, Ni and Cu improve it at 500°C.

This investigation adds to the evidence that the corrosion behaviour of Zircaloy-4 and Zr-2.5 Nb makes them unsatisfactory for high temperature applications; it also shows that the corrosion behaviour of Valoy and Zr-Cr alloys is only marginally better. The most corrosion resistant alloys are Zr-Cu and Zr-Ni. There are too many conflicting results in the literature to establish an effect of steam pressure on the corrosion behaviour of zirconium alloys; however when the published data for the corrosion of Zircaloy-4 (24), Zr-2.5 Nb (25) and Valoy (22, 26) at high pressure are compared with the data of the present study no significant difference is observed. It must be accepted for the present that there may be an appreciable effect of irradiation on the corrosion behaviour of these alloys, although generally irradiation only has an effect below 400°C.

Current corrosion theories for Zr alloys have been adequately discussed by Porte et al. (27), Nomura and Akutsu (28), Dalgaard (29) and Parfenov et al. (30). It is generally believed that Wagner's semiconductor approach to oxidation (31) is not applicable to the majority of zirconium alloy systems because most alloying additions are not sufficiently soluble in α-zirconium. This approach should, however, be applicable to the Zr-Sn and Zr-Nb alloys because Sn and Nb have a reasonably high solubility in Zr at 400 and 500°C, and microprobe studies here

and elsewhere (28, 32, 33) indicate some solubility in the oxide films formed at these temperatures. Because the most likely oxidation valencies of Sn^{3+} and Nb^{3+} are lower than that of Zr^{4+}, they create more rate controlling anion vacancies in the ZrO_2, and as this and other studies have shown, their addition to Zr increases its initial oxidation rate. The oxidation valencies of Fe^{2+}, Cr^{3+}, Ni^{2+}, Cu^{+} and Be^{2+} are also lower than Zr^{4+} but these elements have a neglible solubility in α-zirconium. Furthermore, the microprobe results of this study indicate that Cu and Ni do not enter the oxide and although Fe and Cr do enter they remain as discrete particles. Therefore the defect structure of the corrosion film on Zr-Cr, Zr-Cu, Zr-Fe or Zr-Ni binaries should not be significantly different from that on pure Zr, and these films should be only slightly less protective than pure ZrO_2; this is confirmed in the present study.

The effect of alloying elements on transition and post-transition behaviour cannot be explained so simply. There have been no conclusive experiments to separate the cause from effect of 'breakaway' and the interpretations of this phenomenon and the mode of oxygen transport through 'post-breakaway' films are only speculative.

It has been proposed that extra anion vacancies, although increasing pre-transition corrosion rate, might promote a more ductile oxide film by stress relief (34), and thereby retard the recrystallisation and/or cracking which are two possible causes of 'breakaway' (28, 35). There is no evidence in the present study to confirm this, in fact just the opposite appears to be true, and early 'breakaway' is associated with films which consume significant proportions of low valency alloying additions.

Accelerated transition at higher temperatures has also been attributed to accelerated oxygen diffusion in the oxide underlayer of oxygen-enriched metal. Increased oxygen diffusion in this underlayer may accelerate its growth and embrittlement, and cause a structural change in the adjacent oxide film (36). In the series of corrosion coupons which experienced a temperature transient from 400 to 750°C for 60 hours, the weight gains of the Zr, Zr-Cr, Zr-Fe, Zr-Ni and Zr-Cu alloys were almost identical before and after the temperature transient and the thickness of oxygen-enriched underlayers were also identical after the transient. This indicates no gross differences in rate of diffusion of oxygen in Zr due to Cr, Fe, Ni or Cu additions, so it is unlikely that the early corrosion rate transition of Zr-Cr and Zr-Fe alloys compared with Zr-Cu and Zr-Ni, can be explained by accelerated oxygen diffusion in the underlayer. Simultaneous oxide formation and dissolution can occur on Zr and Zr alloys but oxygen contamination of the metal and its associated embrittlement were not observed at 400 and 500°C in this study. There was, however, considerable evidence for mechanical failure of the underlying oxygen-rich metal which was formed on all

alloy coupons when they experienced the temperature transient to 750°C.

This study gives limited support to the 'stoichiometric change' theory of transition (29) since there was evidence under polarised light of a black oxide, possibly substoichiometric, at the metal/oxide interface, on most zirconium alloys in the post-transition period. The black layer was often outlined by a lateral crack parallel to the metal/oxide interface. Proponents of this theory suggest that thin oxide films on zirconium are non-stoichiometric, less brittle and more protective than the outer stoichiometric layer of thick oxide films.

Correlations of the effects of alloying elements on corrosion properties, with oxide-free energy of formation, atomic or ionic radii and oxide/metal volume ratio have been published (27-30) and data relevant to the present study are given in Table VI. Reference to these data shows that Nb, Sn and Cr differ from Zr more in oxide/metal volume ratio than Ni, Cu and possibly Fe. Furthermore, Nb, Sn and Cr differ from Zr less in oxide-free energy of formation than Ni, Cu and Fe. Although the similarity between this grouping and the corrosion property grouping is probably coincidental, it may be significant that Ni, Cu and Fe oxides are not stable in the presence of Zr ions and tend to form an alloy enriched interfacial layer. The tendency is greater if the additions are less soluble in the oxide than the metal (28, 32). Dalgaard (29) suggested that vacancies may be trapped near these solute rich layers, thereby increasing plasticity at that point to form a ductile barrier against crack propagation. Crack nucleation which relieves compressive stresses in the oxide, may also be related in some way to oxide/metal volume ratio (28, 30).

The corrosion and tensile properties of Zr-2.5 Nb, Zircaloy and Valoy are very sensitive to prior transformation schedule and the possibility of a similar sensitivity in Zr-Cr, Zr-Cu, Zr-Fe and Zr-Ni alloys cannot be disregarded. It is preferable, therefore, to compare alloys in an equivalent metallurgical condition. All corrosion coupons in this study were annealed for 24 hours at 565°C, a treatment which produced similar but not identical metallurgical structures. The treatment did not fully temper the quenched and cold-rolled Zr-Cr, as indicated by the incomplete recovery of its hardness and X-ray line breadth and the dearth of precipitation compared to Zr-Fe, Zr-Cu and Zr-Ni alloys, and this could have been the major reason for the poor corrosion resistance but good tensile properties of the Zr-Cr alloy. Klepfer (39) has progressively improved the corrosion resistance and progressively reduced the tensile strength of Zr-1.15 Cr alloy and Valoy by increasing the annealing temperature from 565 to 788°C, and he claims that corrosion is a function of intermetallic particle size with an optimum at about 1.0 μm diameter. A corrosion study of some modified Zr-Cr, Zr-Ni, Zr-Cu and Zr-Fe alloy structures is in progress. The results so far (Figure 12) indicate a distinct improvement in the corrosion resistance of

Zr-Cr alloy at 500°C by a further anneal at 750°C for 6 hours. Longer corrosion exposures may reveal a similar improvement in Zr-Cu, Zr-Ni and Zr-Fe alloys.

5. CONCLUSIONS

The results of the present investigation suggest that Zircaloy-4, Zr-2.5 Nb and Zr-Cr alloys will not be suitable for service in moist atmospheres at 400-500°C, but Zr-Cu, Zr-Fe and Zr-Ni alloys which have superior corrosion characteristics in this temperature range may be worth considering. The second group of alloys, however, are significantly weaker than the first group although the difference will be smaller at higher temperatures (22). Hydrogen embrittlement, which has not been considered in this study, is known to be a problem in the Zr-Ni alloys, but the problem is less or does not exist in the Zr-Cu and Zr-Fe alloys at 400-500°C (30).

Prior to any transition in the corrosion rate there are only small differences between the corrosion properties of all the alloys, nevertheless, it is possible to correlate these differences with the solubility of alloying elements in the oxide film. The order of decreasing corrosion resistance, prior to transition, appears to follow the order of increasing alloy solubility in the oxide film. It is also interesting to note that the time at which a transition in the corrosion rate occurs and the corrosion rate after transition can be similarly related to the solubility of the alloy addition in the oxide film, the only difference being that Zr-Ni and Zr-Cu alloys are now slightly better than 'pure' Zr. The reason for this difference is unknown, but it may be significant that unlike the other alloying additions considered, copper and nickel have a combination of low negative free energy of formation together with an oxide/metal volume ratio close to that of Zr.

6. ACKNOWLEDGEMENTS

The author is grateful to Mr. E. G. Mehrtens for his assistance with the experimental work, to Mr. F. Scott of the Department of Metallurgy (UNSW) for the electron-beam microprobe analysis and to Mr. E. Mellor for the optical metallography.

7. REFERENCES

(1) Boulton, J. (1969). - AECL-3365.

(2) Greenberg, S. (1964). - Reactor Technology Selected Reviews, p.213.

(3) Lustman, B. and Kerze, F. (1955). - "The Metallurgy of Zirconium", McGraw-Hill Book Company, New York.

(4) Klepfer, H. H., Douglas, D. L. and Armijo, J. S. (1962). - GEAP-3979.

(5) Syre, R. P. (1962). - GEAP-4089 (Vol. 1).

(6) Hausner, H. H. and Kalish, H. S. (1950). - J. Metals, 2, p.59.

(7) Bedford, R. G. (1960). - UCRL-5991-T.

(8) Nielsen, J. W. and Baerziger, N. C. (1954). - Acta. Cryst. 7, p.132.

(9) Hayes, E. T., Roberson, A. H. and Davies, M. H. (1952). - J. Metals, 4, p.304.

(10) Domagala, R. F., McPherson, D. J. and Hansen, M. (1953). - J. Metals, 5, p.279.

(11) Rostaker, W. (1953). - J. Metals, 5, p.304.

(12) Lundin, C. E., McPherson, D. J. and Hansen, M. (1953). - J. Metals, 5, p.273.

(13) Augustson, P. (1950). - USAEC Publ. AECD-3456 (ISC138).

(14) Karlsson, N. (1951). - J. Inst. Metals, 79, p.404.

(15) Pearson, W. B. (1958). - "Lattice Spacings and Structures of Metals and Alloys", Pergamon Press, p.623.

(16) Hayes, E. T., Roberson, A. H. and O'Brian, W. L. (1951). - Trans. Amer. Soc. Met., 43, p.888.

(17) Rhines, F. N. and Gould, R. W. (1963). - Advan. X-Ray Anal., 6, p.62.

(18) Svechnikov, V. N. and Spector, A. T. (1966). - Nucl. Abst., 16, 19388.

(19) Kus'ma, Yu. B., Markiv, V. Ya., Voroshilov, Yu. V. and Skolozdra, R. V. (1966).- Nucl. Sci. Abst. 20, 31727.

(20) Kirkpatrick, M. E. and Larsen, W. L. (1961). - Trans. Amer. Soc. Met. 54, p.580.

(21) Kirkpatrick, M. E., Bailey, D. M. and Smith, J. F. (1962). - Acta. Cryst., 15, p.252.

(22) Klepfer, H. H. (1964). - GEAP-4504.

(23) Gray, D. L. (1961). - AEC R and D Report No. HW-69679.

(24) Kass, S. (1968). - WAPD-TM-782.

(25) Klepfer, H. H. (1963). - J. Nucl. Mat. 9, (1), p.65.

(26) Klepfer, H. H., Baroch, C. J., Blood, R. E., Jaech, J. L. and Pickett, E. A. (1965). - GEAP-4840.

(27) Porte, H. A., Schnizlein, J. G., Vogel, R. G. and Fischer, D. F. (1960). - J. Electrochem. Soc., 107, (6), p.506.

(28) Sueo Nomura and Cho Akutsu, (1966). - Electrochem. Tech., 4, No. 3-4, p.93.

(29) Dalgaard, S. B. (1962). - AECL-1513.

(30) Parfenov, B. G., et al. (1969). - AEC.-tr-6978.

(31) Kubaschewski, O. and Hopkins, B. E. (1953). - "Oxidation of Metals and Alloys", Butterworths Scientific Publications, London.

(32) Greenbank, J. C. and Harper, S. (1966). - Electrochem. Tech., 4, (No. 3-4), p.142.

(33) Douglas, D. L. (1965). - Corrosion Science, 5, p.347.

(34) Douglas, D. L. (1965). - Corrosion Science, 5, p.255.

(35) Cox, B. (1969). - J. Nucl. Mat., 29, p.50.

(36) Pemsler, J. P. (1966). - J. Electrochem. Soc., 113, (12) p.1241.

(37) Cottrell, A. H. (1967). - "An Introduction to Metallurgy", Edward Arnold (Publishers) Ltd., London, p.35-37.

(38) "Handbook of Chemistry and Physics" (1959). - Chemical Rubber Publishing Co, U.S.A. 41st Edition.

(39) Klepfer, H. H., Blood, R. E. and Jaech, J. L. (1966). - GEAP-5065.

TABLE I

CRYSTALLOGRAPHIC DATA FOR ZIRCONIUM-RICH INTERMETALLICS

Intermetallic Compound	Crystal Structure	Lattice Parameters (Å)		Nos. of Molecules in a unit cell	Calculated Density (g/cm^3)
		a	c		
$ZrCr_2$	Hexagonal	5.182	8.429	4	6.61
Zr_2Fe	Tetragonal	6.457	5.542	4	6.84
Zr_2Cu	Tetragonal	3.3	11.3	2	6.64
Zr_2Ni	Tetragonal	6.477	5.241	4	7.28
$ZrBe_2$	Hexagonal	3.82	3.24	1	4.43

TABLE II

ZIRCONIUM ALLOY COMPOSITIONS

Alloy	Weight per cent Addition		H_2 (p.p.m.)	N_2 (p.p.m.)
	Nominal	Analysed		
Iodide Zr	-	-	52	159
Zircaloy-4	Fe 0.2, Cr 0.1, Sn 1.5	Fe 0.22, Cr 0.1, Sn 1.54	57	166
Nb-Zr	Nb 2.5	Nb 2.43	53	123
Valoy	Cr 1.15, Fe 0.1	Cr 1.32, Fe 0.14	46	78
Cr-Zr	Cr 1.15	Cr 1.23	67	110
Fe-Zr	Fe 0.53	Fe 0.54	73	132
Cu-Zr	Cu 0.56	Cu 0.59	91	150
Ni-Zr	Ni 0.58	Ni 0.69	48	170
Be-Zr	Be 0.24	Be 0.29	64	119

TABLE III

CORROSION RESULTS

Alloy	Corrosion Temp. °C	t_o (hr)	n_1	Weight Gain at t_o (mg/dm^2)	Post Transition Corrosion Rate (m.d.d.)	n_2
Zr	400	-	0.45	-	-	-
	500	3620	0.53	172	2.28	1.51
Zr-4	400	1000	0.36	43	0.79	0.86
	500	322	0.39	92	11.9	1.35
Nb-Zr	400	1420	0.52	76	1.3	0.99
	500	135	0.53	88	10.6	0.84
Valoy	400	3600	0.41	69	0.41	0.94
	500	395	0.40	69	4.85	1.05
Cr-Zr	400	1600	0.41	51	0.62	0.88
	500	460	0.41	84	3.27	0.90
Fe-Zr	400	6500	0.46	94	0.24	0.77
	500	3200	0.46	240	3.55	1.53
Cu-Zr	400	-	0.41	-	-	-
	500	4900	0.42	190	0.84	1.00
Ni-Zr	400	-	0.39	-	-	-
	500	4800	0.42	185	0.97	1.00
Be-Zr	400	7000	0.46	62	0.21	1.00
	500	1310	0.46	92	2.44	1.18

TABLE IV

PARTICLE SIZE ANALYSIS OF SPECIMENS ANNEALED 24 HR AT 565°C PLUS 6 HR AT 750°C

Alloy	Volume Fraction of Intermetallic		Particle Size (μm)	
	Calculated	Measured	Mean	Maximum
Zr + Cr 1.23	0.023	0.022	0.06	0.15
Zr + Fe 0.54	0.022	0.031	0.15	0.35
Zr + Cu 0.59	0.022	0.033	0.30	0.70
Zr + Ni 0.69	0.025	0.020	0.70	1.60
Zr + Cr 1.32 + Fe 0.14	0.030	0.040	0.10	0.20

TABLE V

MECHANICAL PROPERTIES OF ALLOYS, HOT-ROLLED, β-QUENCHED, COLD-ROLLED AND TEMPERED

Alloy	Temper Treatment*	Test Temp. °C	Strength (p.s.i.) 0.2% YS	UTS	Total Elong. %
IODIDE ZIRCONIUM	A	25	21,100	31,950	31.4
		300	9,400	15,400	28.7
	B	25	17,930	28,150	32.0
		300	7,250	11,130	31.6
Zr + 1.15 Cr	A	25	46,900	89,200	13.5
		300	28,200	42,800	9.5
	B	25	24,400	45,500	28.3
		300	11,250	26,600	30.8
Zr + 0.53 Fe	A	25	33,700	53,575	21.0
		300	21,300	29,300	19.5
	B	25	24,500	44,500	33.2
		300	10,560	23,200	32.3
Zr + 0.56 Cu	A	25	33,400	50,500	24.9
		300	18,800	27,900	25.4
	B	25	27,800	44,300	31.5
		300	9,600	22,200	42.6
Zr + 0.58 Ni	A	25	30,900	50,800	20.6
		300	21,300	29,200	22.4
	B	25	26,350	44,000	28.3
		300	9,950	20,600	28.4

* Temper Treatment A - 24 hours at 565°C

B - 6 hours at 750°C

TABLE VI

SOME PROPERTIES OF THE ALLOYING ELEMENTS COMPARED TO THOSE OF Zr

Alloy Addition and most likely Oxidation valency	Atomic Radius (Å)	Ionic Radius (Å)	Approximate ΔF (k cal) for oxide at 25°C	Ratio of $\frac{\text{oxide volume}}{\text{metal volume}}$
Be^{+2}	1.13	0.34	-139	1.68
Cr^{+3}	1.25	0.75	-250	2.07
Fe^{+2}	1.24	0.83	- 58	1.73
Ni^{+2}	1.25	0.78	- 52	1.65
Cu^{+1}	1.27	0.96	- 35	1.64
Zr^{+4}	1.60	0.80	-244	1.56
Nb^{+2}	1.42	0.79	- 85	1.37
Sn^{+4}	1.58	0.74	-124	1.32

Data compiled from references (27) (28) (29) (31) (37) and (38).

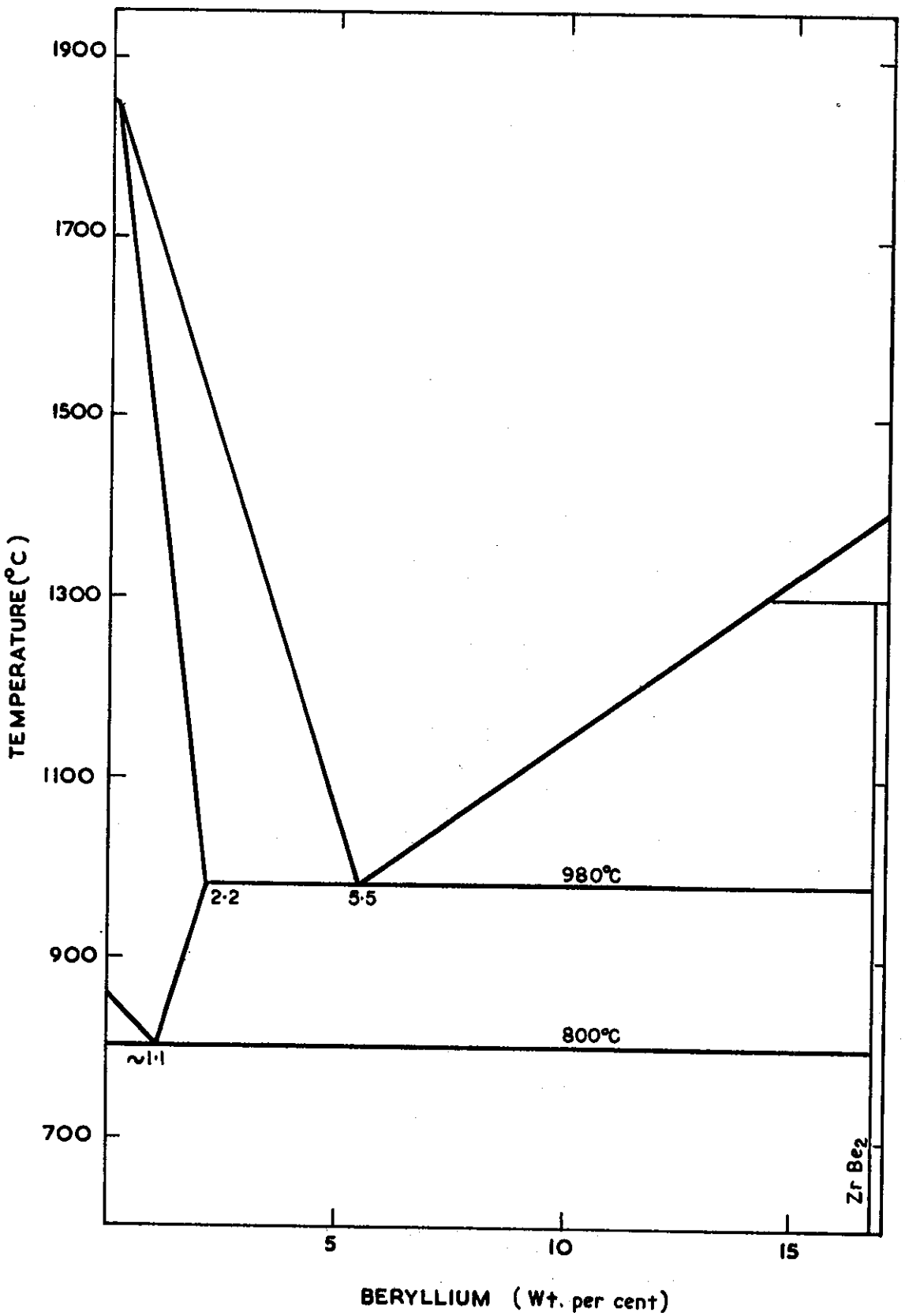

FIGURE 1. ZIRCONIUM - BERYLLIUM SYSTEM

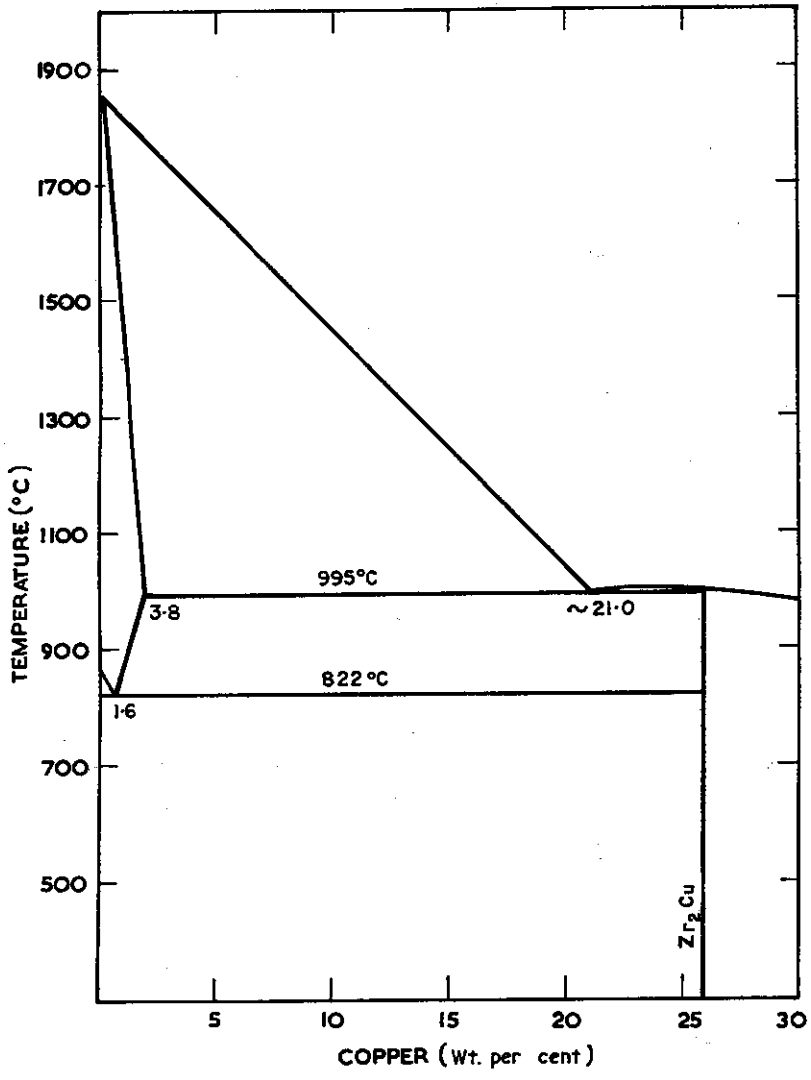

FIGURE 2. ZIRCONIUM - COPPER SYSTEM

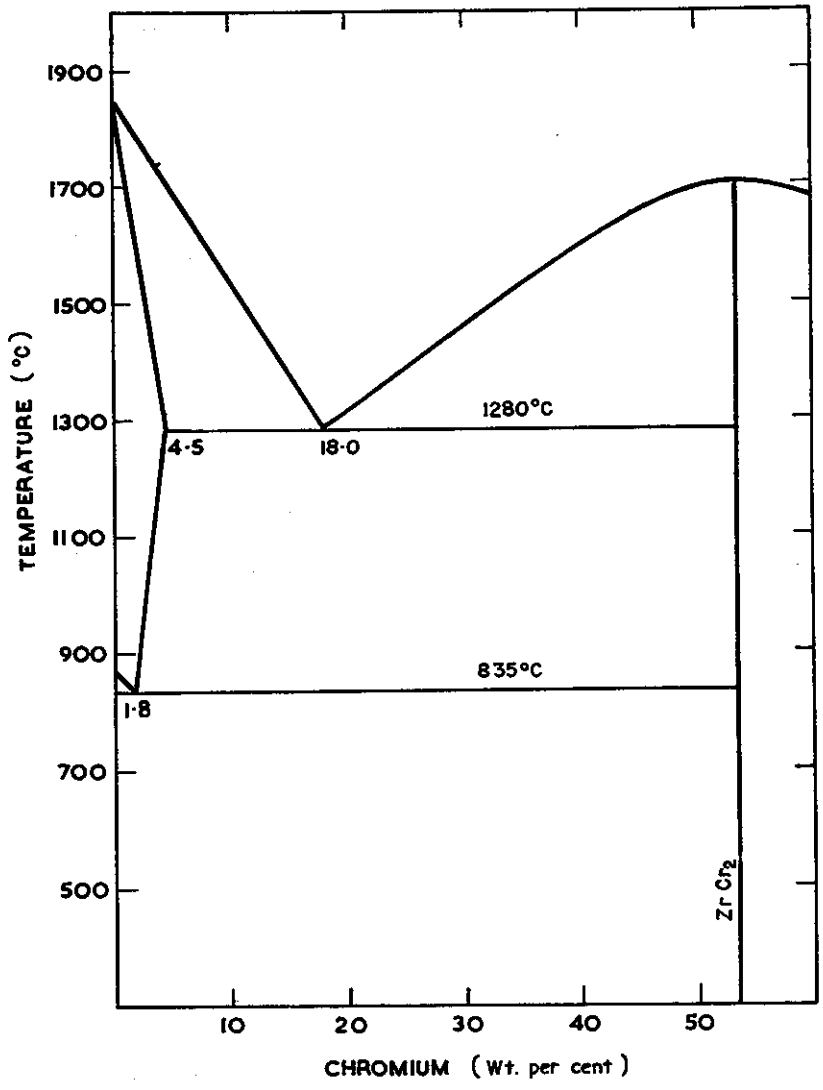

FIGURE 3. ZIRCONIUM - CHROMIUM SYSTEM

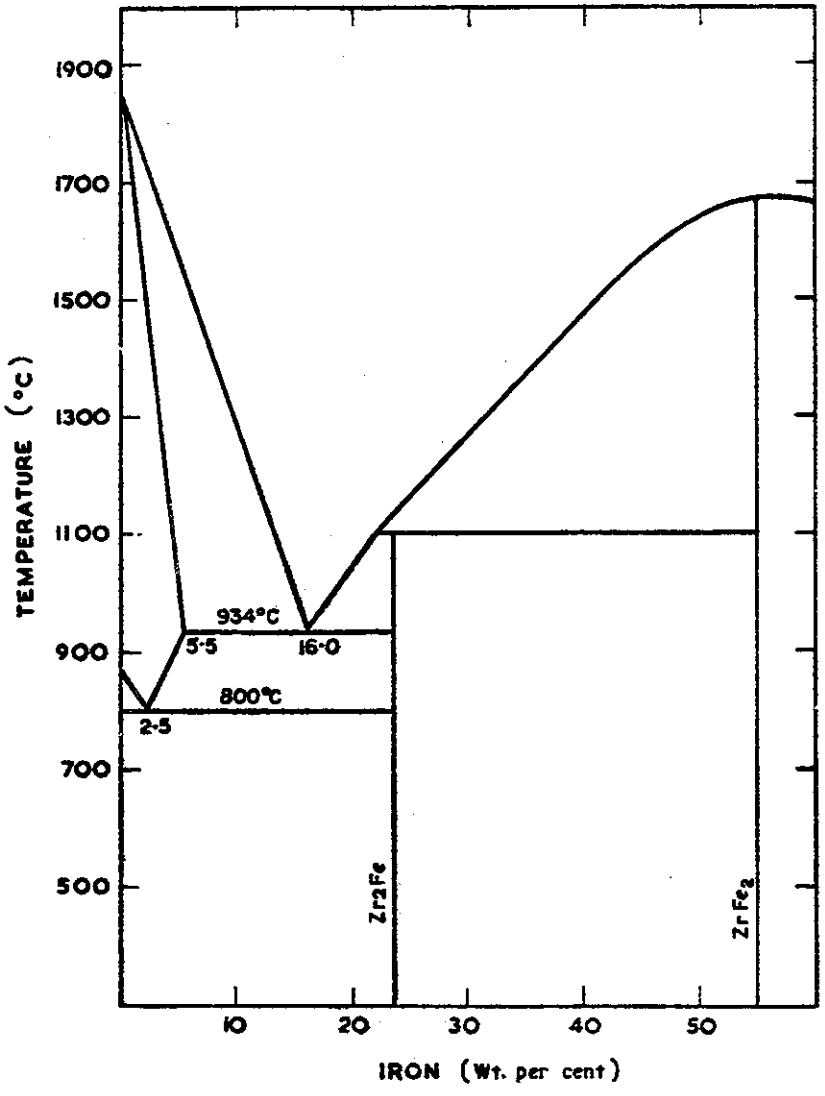

FIGURE 4. ZIRCONIUM - IRON SYSTEM

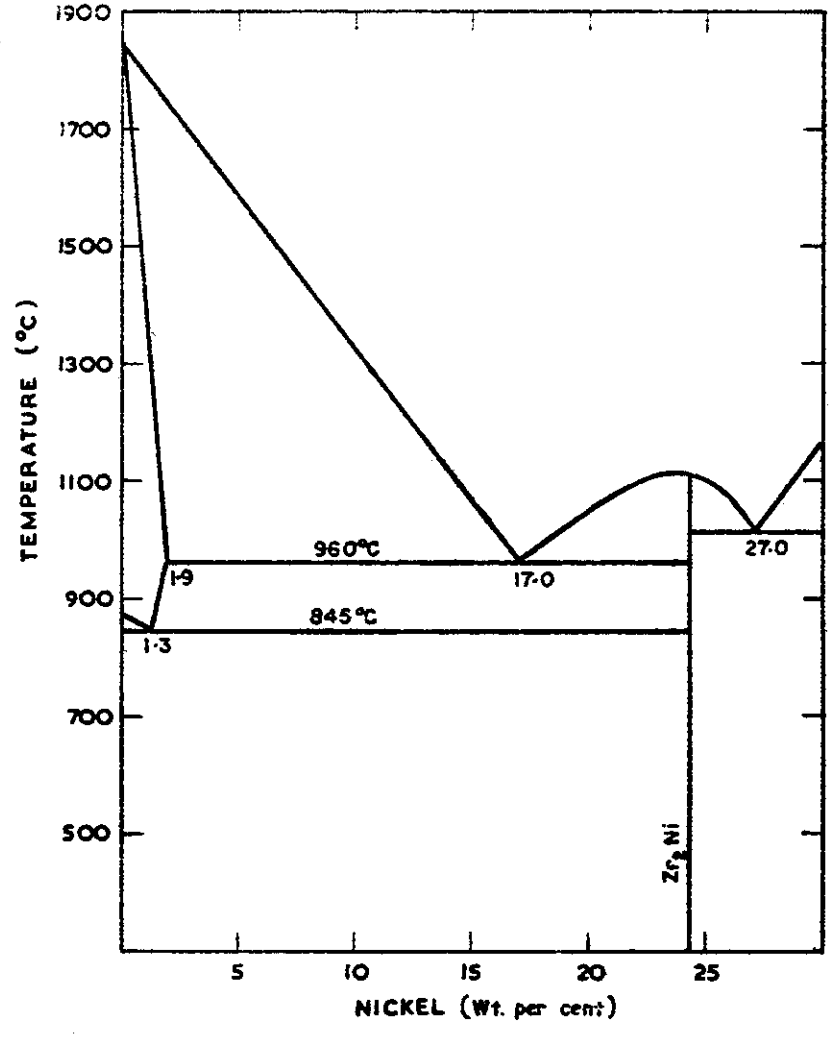

FIGURE 5. ZIRCONIUM - NICKEL SYSTEM

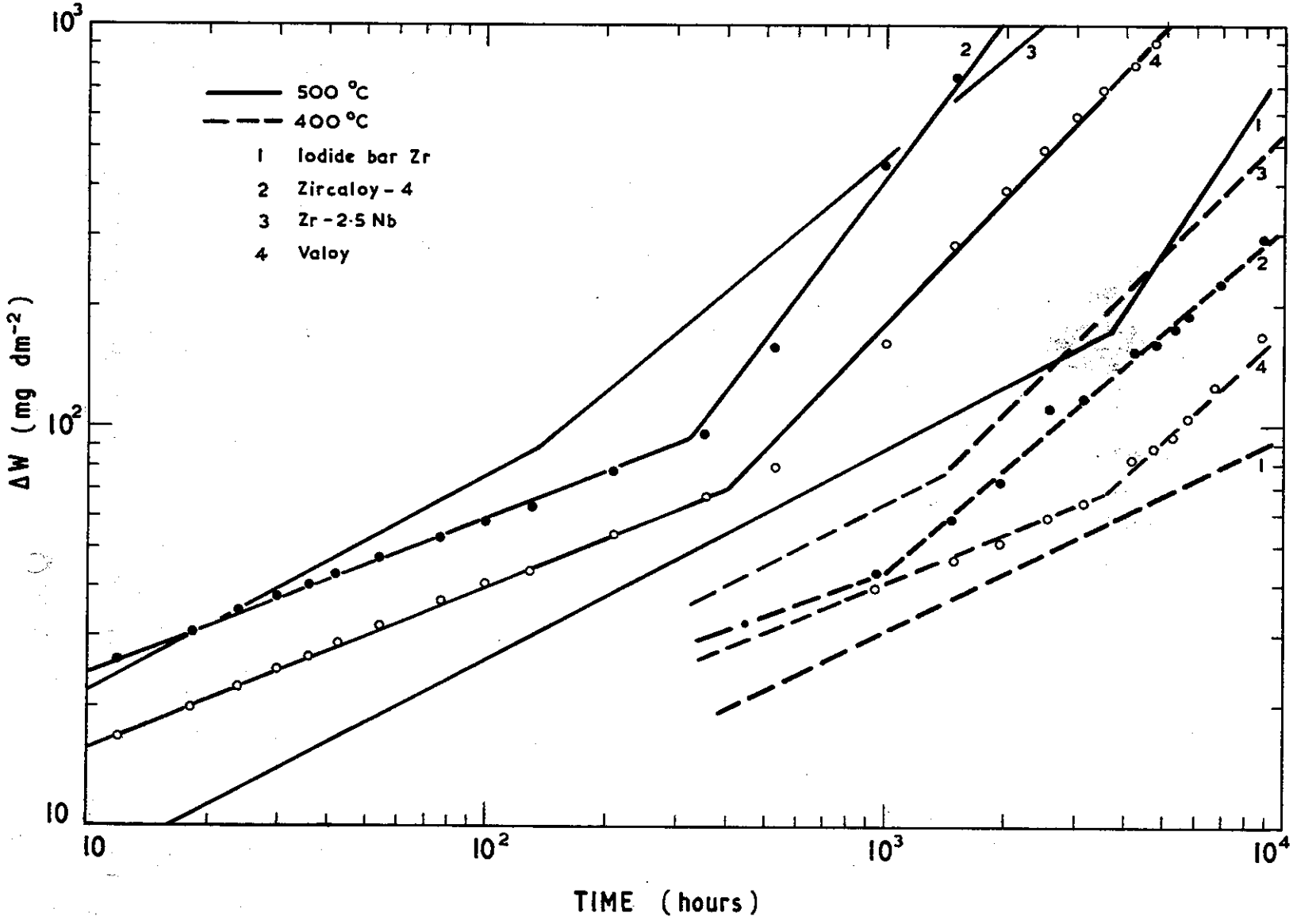

FIGURE 6. CORROSION IN MOIST HELIUM OF ZIRCONIUM, ZIRCALOY-4, Zr-2.5 Nb AND 'VALOY'

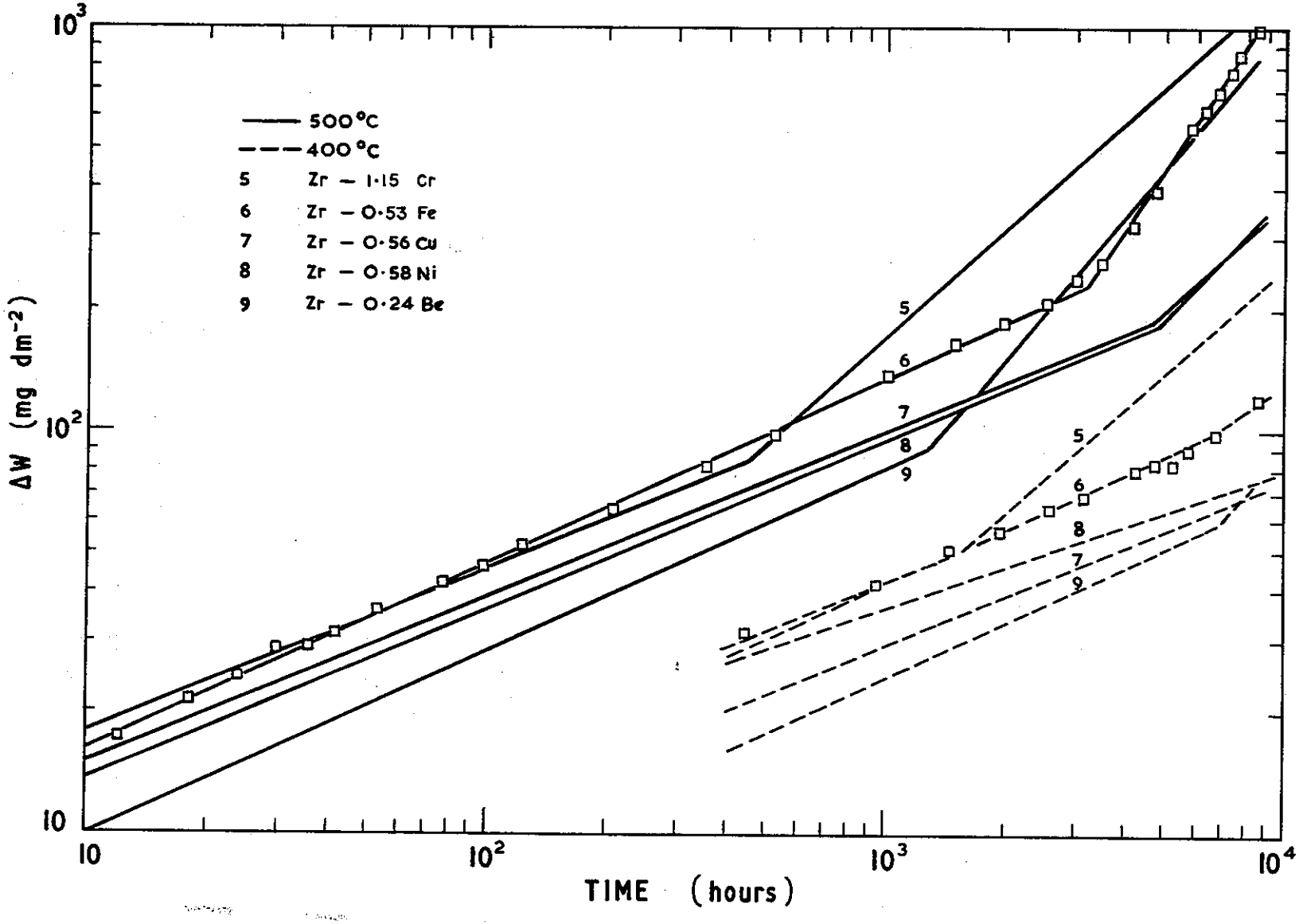

FIGURE 7. CORROSION IN MOIST HELIUM OF Cr, Cu, Be, Fe AND Ni ZIRCONIUM BASED ALLOYS

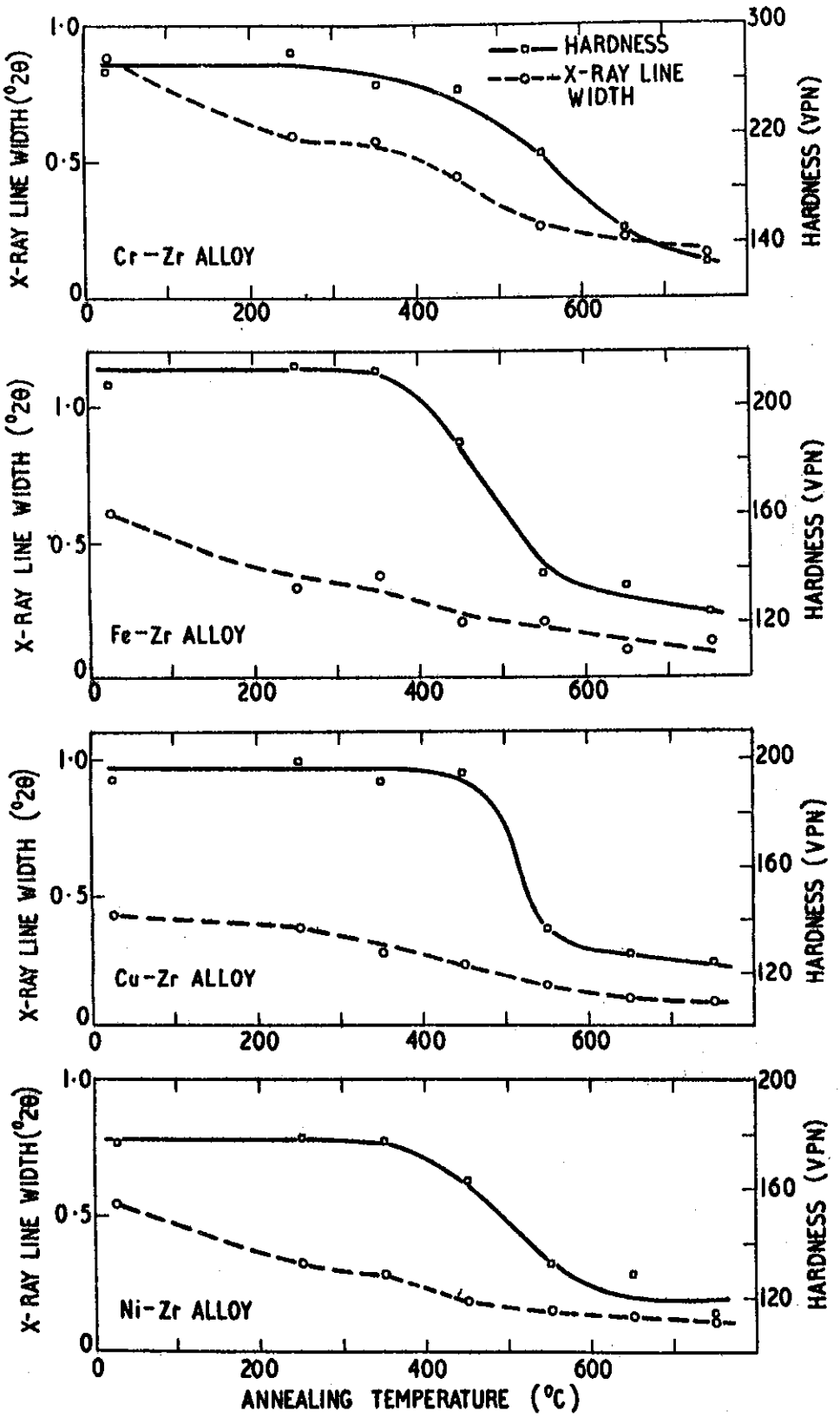

FIGURE 8. X-RAY LINE WIDTH OF THE (213) Kα DOUBLET AND HARDNESS FOR SOME BETA-QUENCHED AND 20 PER CENT COLD-ROLLED ALLOYS ANNEALED FOR 18 HOURS

25°C

550°C

750°C

FIGURE 9a. 'PURE' Zr BETA QUENCHED, COLD ROLLED 20%, ANNEALED 18hrs 550°C AND 750°C
(POL. LIGHT X100)

25°C

550°C

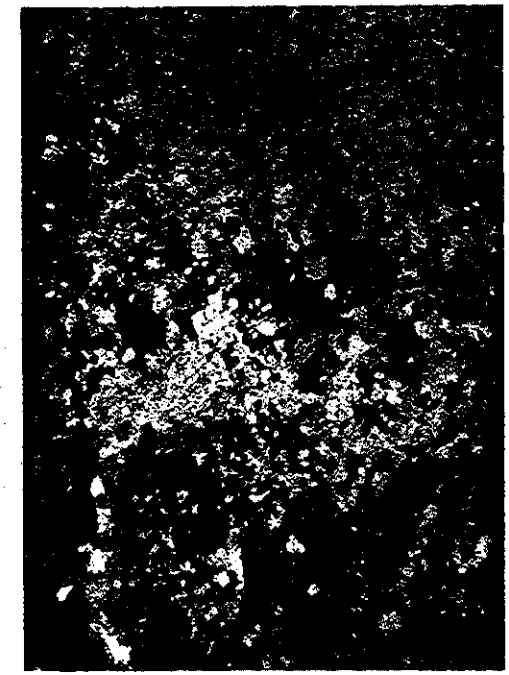

750°C

FIGURE 9b. Zr + 0.53 Fe BETA QUENCHED, COLD ROLLED 20%, ANNEALED 18 hrs 550°C AND 750°C (POL. LIGHT X100)

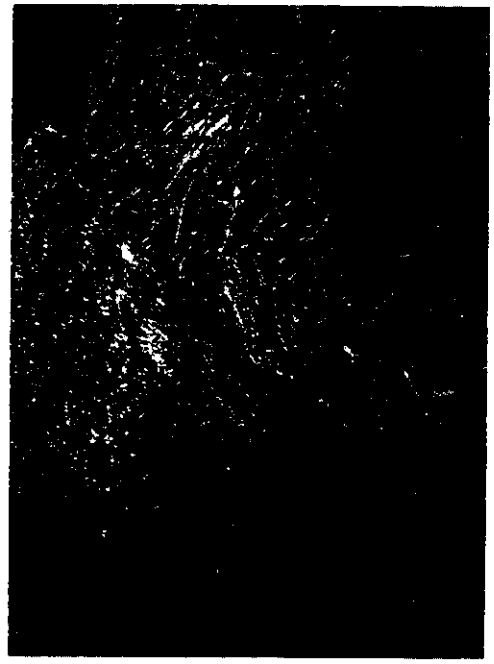

25°C

550°C

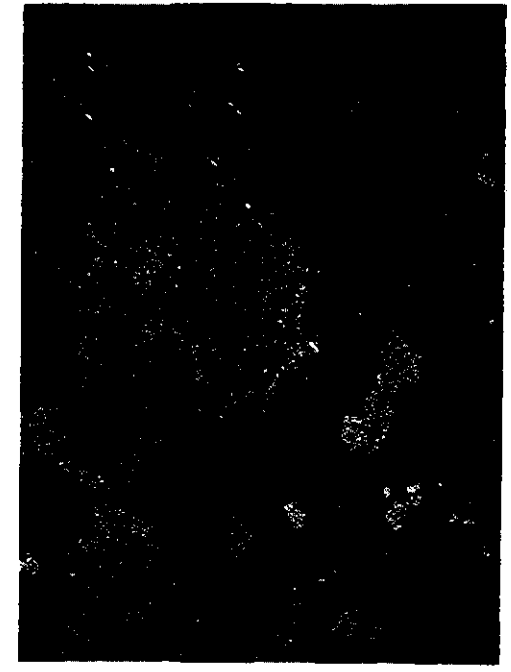

750°C

FIGURE 9c. Zr + 1.15 Cr BETA QUENCHED, COLD ROLLED 20%, ANNEALED 18 hrs 550°C AND 750°C (POL. LIGHT X100)

PURE Zr

Zr + 0.58 Ni

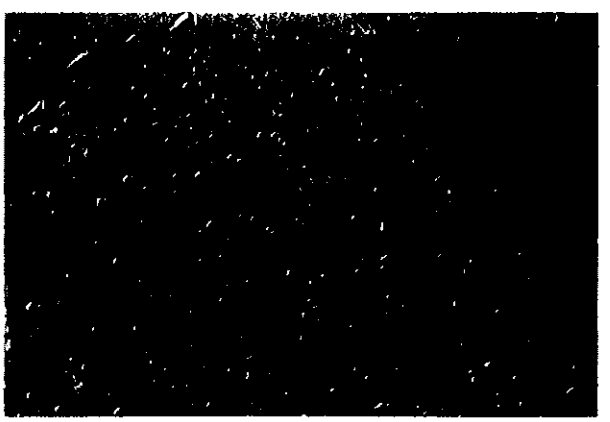

Zr + 0.53 Fe

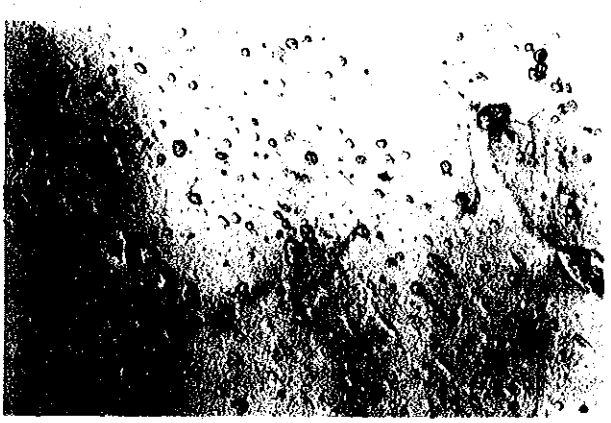

Zr + 0.56 Cu

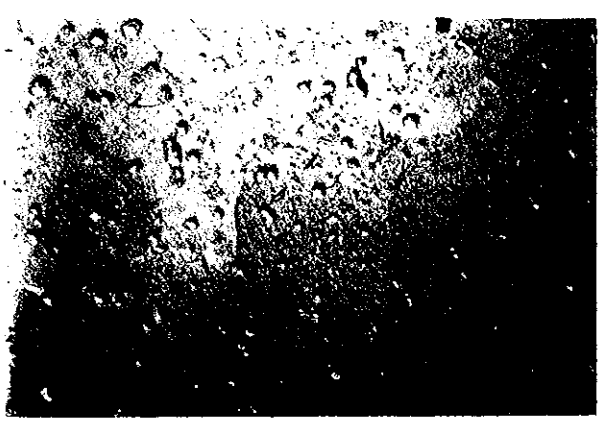

Zr + 1.15 Cr

FIGURE 10. ELECTRON PHOTOMICROGRAPHS OF SOME ANNEALED ZIRCONIUM ALLOYS (X4000)

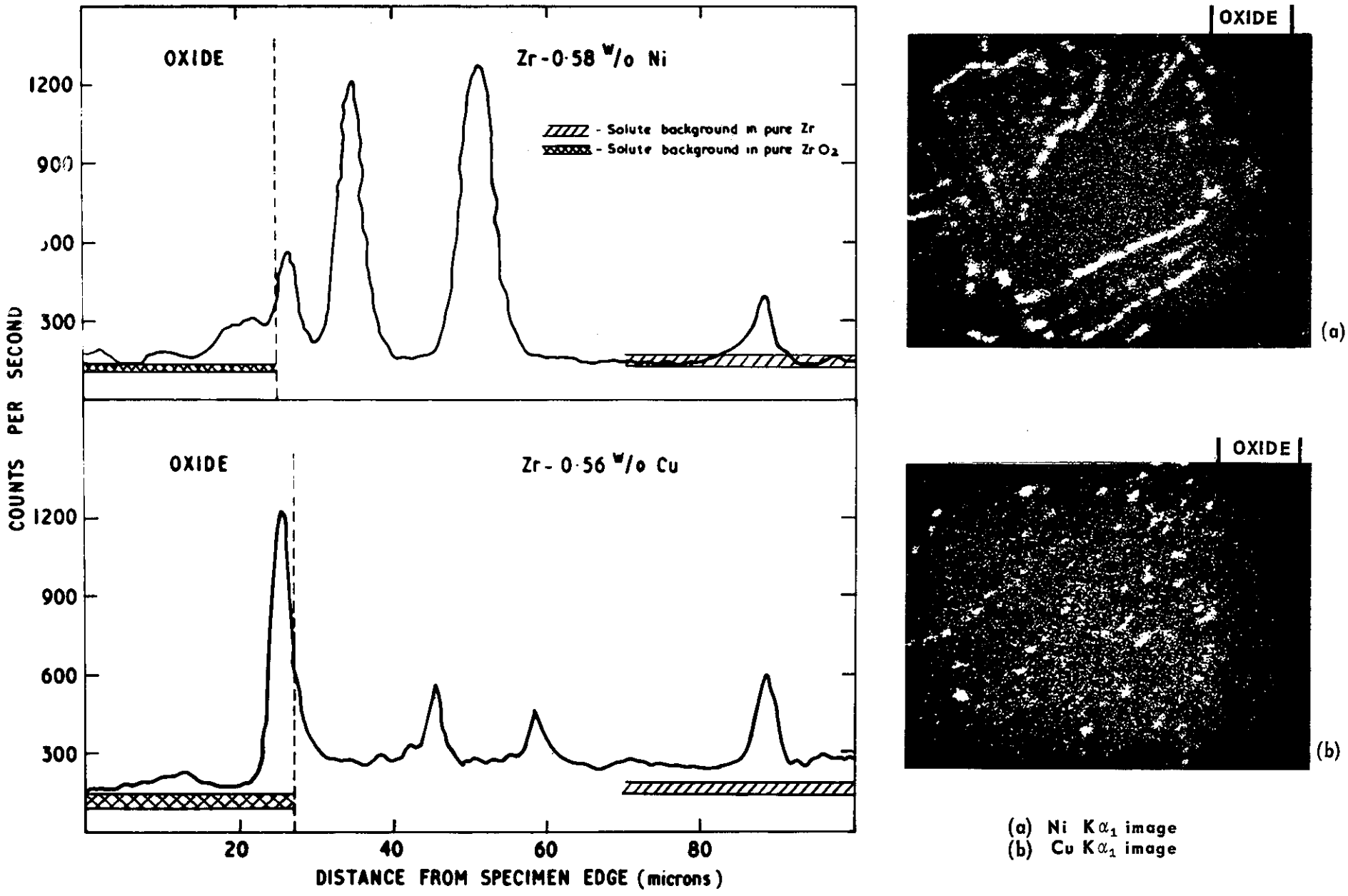

FIGURE 11a. SOLUTE DISTRIBUTION BETWEEN ZIRCONIUM ALLOYS AND OXIDE FILMS FORMED AT 500°C

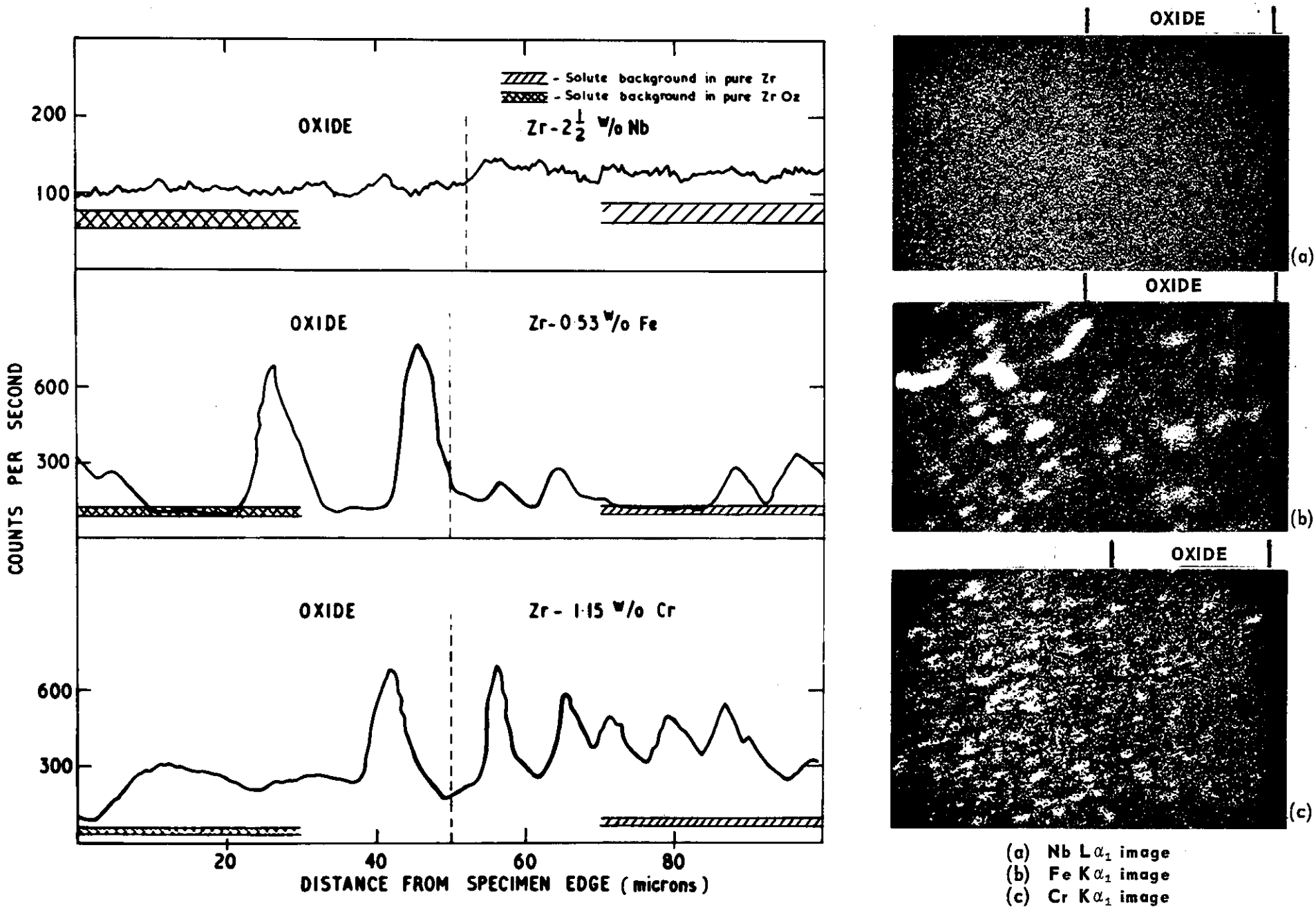

(a) Nb $L\alpha_1$ image
(b) Fe $K\alpha_1$ image
(c) Cr $K\alpha_1$ image

FIGURE 11b. SOLUTE DISTRIBUTION BETWEEN ZIRCONIUM ALLOYS AND OXIDE FILMS FORMED AT 500°C

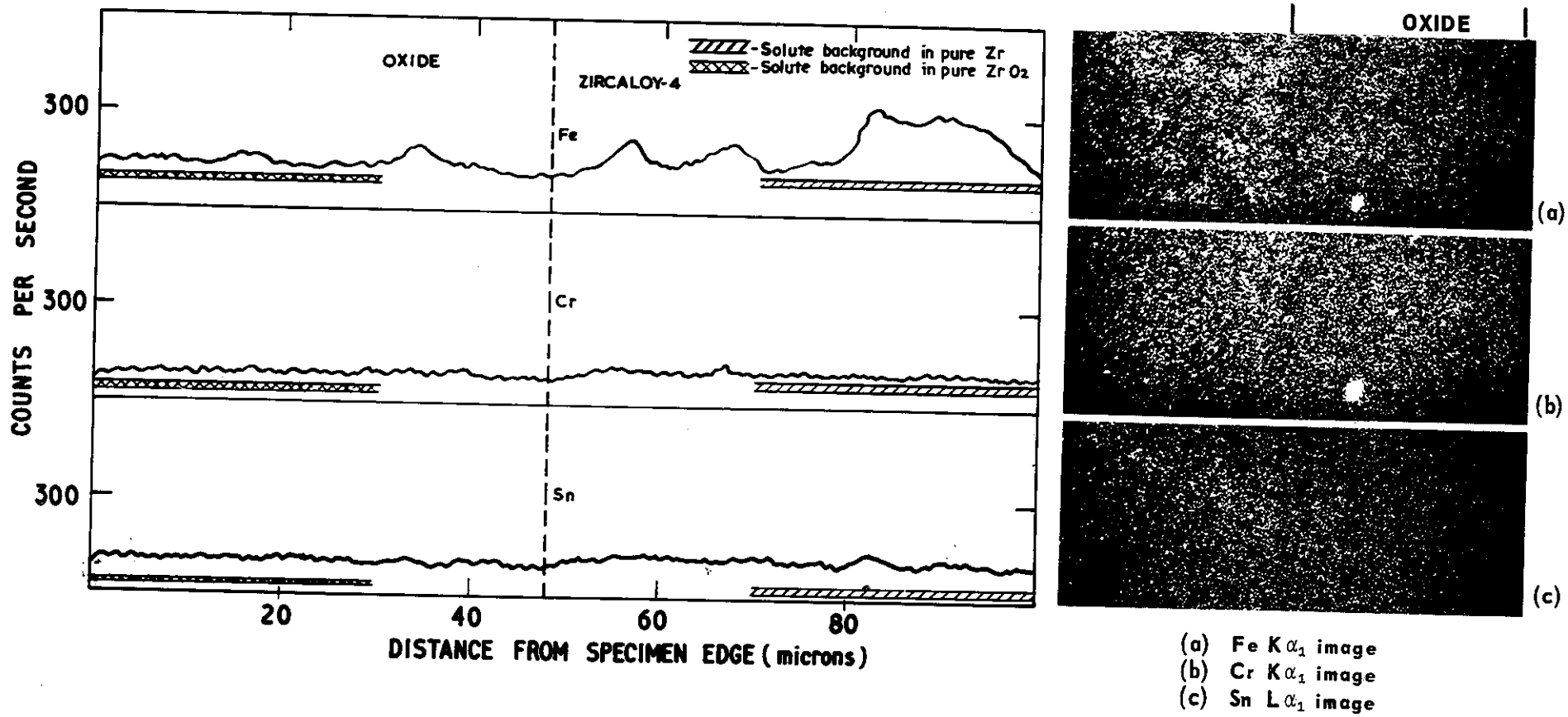

FIGURE 11c. SOLUTE DISTRIBUTION BETWEEN ZIRCONIUM ALLOYS AND OXIDE FILMS FORMED AT 500°C

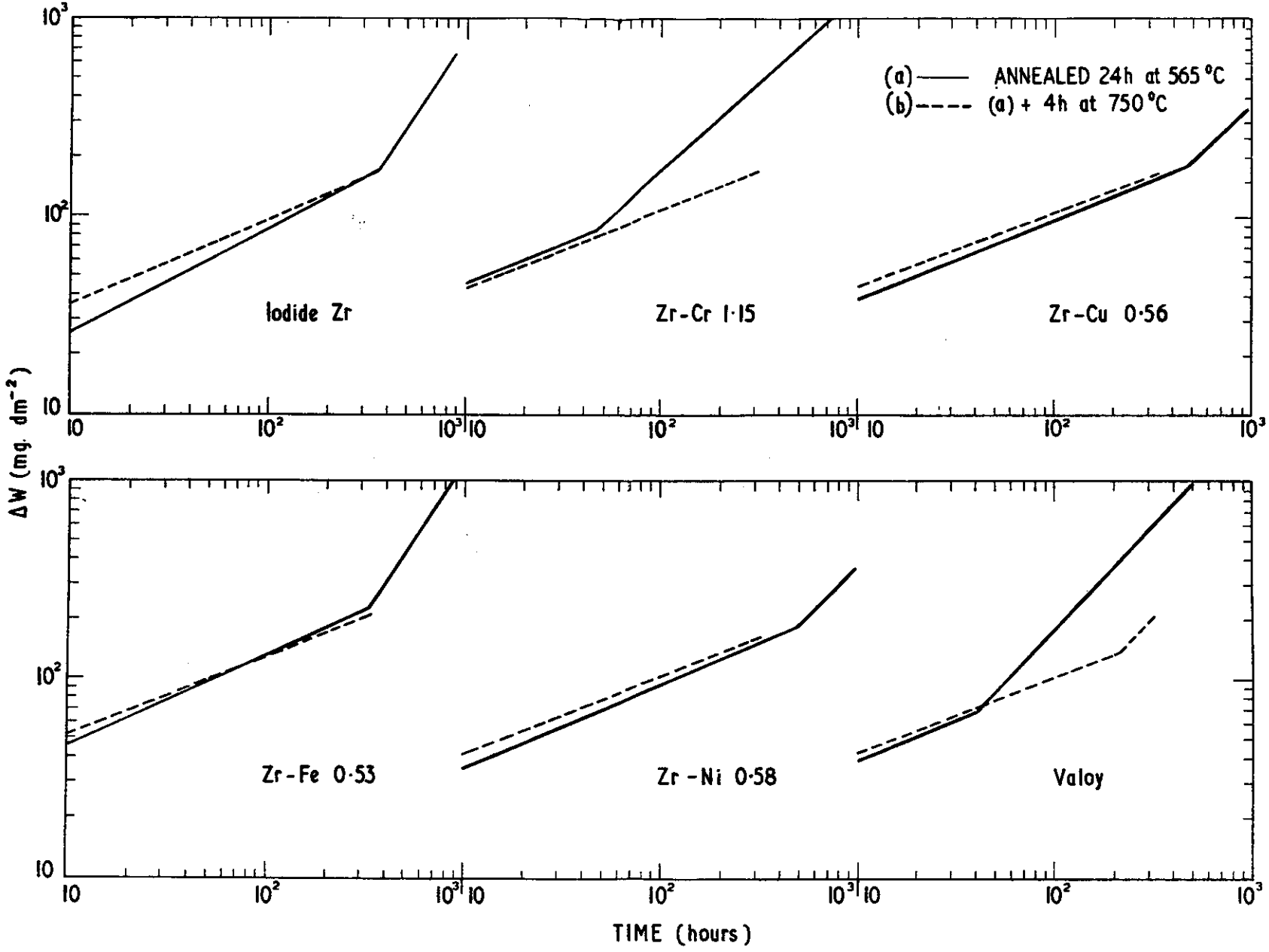

FIGURE 12. EFFECT OF ANNEALING ON THE CORROSION OF ZIRCONIUM ALLOYS AT 500°C